Observations of carbon export by small sinking particles in the upper mesopelagic

Colleen A. Durkin *, Margaret L. Estapa [1], Ken O. Buesseler

Woods Hole Oceanographic Institution, 266 Woods Hole Road, Woods Hole, MA 02543, United States

ABSTRACT

Carbon and nutrients are transported out of the surface ocean and sequestered at depth by sinking particles. Sinking particle sizes span many orders of magnitude and the relative influence of small particles on carbon export compared to large particles has not been resolved. To determine the influence of particle size on carbon export, the flux of both small (11–64 μm) and large (>64 μm) particles in the upper mesopelagic was examined during 5 cruises of the Bermuda Atlantic Time Series (BATS) in the Sargasso Sea using neutrally buoyant sediment traps mounted with tubes containing polyacrylamide gel layers and tubes containing a poisoned brine layer. Particles were also collected in surface-tethered, free-floating traps at higher carbon flux locations in the tropical and subtropical South Atlantic Ocean. Particle sizes spanning three orders of magnitude were resolved in gel samples, included sinking particles as small as 11 μm. At BATS, the number flux of small particles tended to increase with depth, whereas the number flux of large particles tended to decrease with depth. The carbon content of different sized particles could not be modeled by a single set of parameters because the particle composition varied across locations and over time. The modeled carbon flux by small particles at BATS, including all samples and depths, was 39 ± 20% of the modeled total carbon flux, and the percentage increased with depth in 4 out of the 5 months sampled. These results indicate that small particles (<64 μm) are actively settling in the water column and are an important contributor to carbon flux throughout the mesopelagic. Observations and models that overlook these particles will underestimate the vertical flux of organic matter in the ocean.

© 2015 The Authors. Published by Elsevier B.V. This is an open access article under the CC BY-NC-ND license (http://creativecommons.org/licenses/by-nc-nd/4.0/).

1. Introduction

The biological pump leads to the uptake and sequestration of carbon by the ocean (Volk and Hoffert, 1985). The first step of the biological pump occurs when phytoplankton fix inorganic carbon into organic matter in the surface ocean, and the last step occurs when organic carbon sinks or is subducted into the deep ocean and is removed from contact with the atmosphere. Organic carbon is transported out of the surface ocean by particles, which include organisms, organic aggregates, and fecal pellets. Whether those particles reach the deep ocean before their carbon is consumed or respired depends on their individual characteristics and the influence of ecological processes as they sink through the mesopelagic zone (Buesseler et al., 2007b; De La Rocha and Passow, 2007). The amount of carbon that reaches the deep ocean is ultimately determined at the scale of the individual particle, so characterization of sinking particles and their ecological role is needed to determine the underlying mechanisms of carbon uptake by the ocean.

The size of a particle influences its fate as it sinks through the water column (Stemmann and Boss, 2012; Woodward et al., 2005), and for decades, great effort has gone toward identifying the particle size range contributing the most to carbon export (Dall'Olmo and Mork, 2014; Fowler and Knauer, 1986; Jacobs et al., 1973; McCave, 1975; Michaels and Silver, 1988; Richardson and Jackson, 2007; Riley et al., 2012). According to Stokes' Law, particle sinking speed scales with the square of particle size, and therefore large particles sink faster and are more likely to reach the deep ocean before being remineralized by bacteria. The importance of large particles (>100 μm) in transporting carbon to the deep ocean has been observed in multiple ocean environments (Guidi et al., 2009; Jackson et al., 2005; Riley et al., 2012) and explored in export models (Buesseler and Boyd, 2009; Giering et al., 2014; Siegel et al., 2014; Stemmann et al., 2004b). Observing small particles (<100 μm) at the same time as large particles is a methodological challenge because no single instrument or sampling device can resolve the entire size range of particles present in the water column (Jackson and Burd, 1998; Stemmann and Boss, 2012). Only a few studies have quantified suspended particle sizes spanning three orders of magnitude by combining instruments (Jackson et al., 1997; Stemmann et al., 2008). Differentiating sinking small particles from suspended small particles is even more challenging, and it is often assumed that small particles do not sink or sink so slowly that they are respired in the upper mesopelagic (Giering et al.,

* Corresponding author.
  E-mail address: cdurkin@whoi.edu (C.A. Durkin).
[1] Present address: Skidmore College, 815 N. Broadway, Saratoga Springs, NY 12866, United States.

2014; Riley et al., 2012). These assumptions should be re-evaluated, since settling of small particles down to 1000 m and deeper has been observed (Dall'Olmo and Mork, 2014; Silver and Gowing, 1991).

Fast sinking speeds may not be required for small particles to contribute significantly to carbon export. In the Mediterranean Sea, the subarctic Pacific, and the subtropical North Pacific, approximately 50% of the carbon flux was attributed to particles sinking less than 100 m per day (Trull et al., 2008). During multiple sediment trap deployments near the Canary Islands, the largest fraction of bulk carbon flux was attributed to particles sinking between 0.7 and 5 m per day (Alonso-González et al., 2010). Although the size of these slowly sinking particles is unknown, particles sinking at these rates would either be small or have low density.

Small particles may be transported to depth at rates exceeding their own gravitational settling speeds through aggregation or because of physical mixing. Aggregates formed from small particles at the surface may sink below the surface layer rapidly and disaggregate at depth (Burd and Jackson, 2009; Jackson and Burd, 1998; Stemmann et al., 2004a). Several studies that combine modeling with particle measurements have concluded that small particles are transported to the deep sea by this mechanism of aggregation and disaggregation (Close et al., 2013; Giering et al., 2014; Richardson and Jackson, 2007; Stemmann et al., 2004a). This mechanism agrees with the established view that particles must be large to contribute to carbon flux, because the small particles in these models are exported only when part of larger aggregates. Alternatively, small particles could be transported by the "mixed layer pump", in which deep winter mixing transports small particles to depth and spring/summer shoaling of the mixed layer isolates these particles from the surface (Gardner et al., 1995). The mixed-layer pump was one of the proposed mechanisms for the observed vertical transport of particles smaller than 20 μm down to 1000 m in the Norwegian Sea (Dall'Olmo and Mork, 2014). Neither aggregation nor the mixed layer pump requires gravitational settling by individual small particles in order for them to contribute to carbon export.

Alternatively, small particles might be capable of sinking through the water column if shape and excess density contribute to enhanced settling speeds. McDonnell and Buesseler (2010, 2012) measured the sinking speed of various particle size classes in both the Southern Ocean and the Sargasso Sea, and found that smaller particles generally had slower sinking speeds than larger particles, as predicted by Stokes Law. However, they found an exception for the smallest observed particles (73–195 μm), which had faster sinking speeds than some of the larger particles. This apparent departure from Stokes Law was possible due to variation in the shape and density of different particle size classes, but the authors' observations did not extend to smaller particles (<73 μm) below the resolution of their observational techniques. If small particles sink faster than expected, they may have an unanticipated contribution to carbon export.

Small particles may contribute significantly to carbon flux due to aggregation and disaggregation, physical mixing, or direct gravitational settling. In the present study, we quantify the flux of both small and large particles in the Sargasso Sea and at various locations in the southern subtropical and tropical Atlantic Ocean with the use of polyacrylamide gels placed in the bottom of sediment traps, referred to here as gel traps (Ebersbach and Trull, 2008; Lundsgaard, 1995; McDonnell and Buesseler, 2010; Waite et al., 2000). Sinking particles gently settle into the gel layer at the bottom of the trap tube, retaining their original characteristics and maintaining their separation from one another. We observe sinking particles from a larger size range than in previous gel trap studies and quantify sinking particles as small as 11 μm. Particles that settle into the gel trap are by definition sinking, thus the fluxes we calculate are due to the sinking of individual particles at the depth at which they were collected. We calculate the contribution of both small (here defined as 11–64 μm) and large particles (>64 μm) to total carbon flux as they sink out of the surface and through the mesopelagic ocean.

2. Methods

2.1. Preparation of polyacrylamide gels

Polyacrylamide gel layers were prepared in 11 cm diameter polycarbonate jars (Thermo Fisher Scientific Inc., USA) using methods described in previous studies (Ebersbach and Trull, 2008; Lundsgaard, 1995; McDonnell and Buesseler, 2010) with slight modifications. To prepare 12% polyacrylamide gel, 7.5 g of sea salts (Sigma-Aldrich, USA) was dissolved into 400 mL of surface seawater from Vineyard Sound, MA, USA and filtered through a 0.2 μm polycarbonate filter (Millipore, Thermo Fisher Scientific Inc., USA). The filtered brine was boiled for 15 min to reduce the oxygen content and reduce the brine volume to 350 mL. The solution was bubbled with nitrogen gas through glass pipet tips attached to a pressurized tank while the solution cooled to room temperature. The container of brine was then placed in an ice bath on a stir plate and 150 mL of 40% acrylamide solution (Thermo Fisher Scientific Inc., USA) and 1 g of ammonium persulfate (Thermo Fisher Scientific Inc., USA) was added to the solution while stirring. After the ammonium persulfate dissolved, 1 mL of tetramethylethylenediamine (Acros Organics, Thermo Fisher Scientific Inc., USA) was added to catalyze polymerization. The gel jars deployed in ballasted, neutrally buoyant sediment traps were required to weigh 140 g. To achieve consistent weights, a large volume of polyacrylamide gel was prepared and then poured into each jar. Gels were stored at 4 °C until use.

2.2. Particle collection

Samples were collected during five Bermuda Atlantic Time Series (BATS) cruises in the western Sargasso Sea in July, August, September, and October 2013 and in March 2014 aboard the R/V Atlantic Explorer (Fig. 1). Neutrally buoyant sediment traps (NBSTs) (Valdes and Price, 2000) with modified burn-wire closure mechanisms were deployed at three depths for approximately 3 days during each cruise (Table 1). The polycarbonate trap tubes were 12 × 70 cm with a collection diameter of 0.0133 m². Four samples were collected in the southern subtropical and tropical Atlantic during March–May 2013 on the DeepDOM cruise aboard the R/V Knorr (1 deployment at Station 2, 2 deployments

Fig. 1. Map of locations where sediment traps were deployed.

Table 1
Summary of sediment trap deployments, measured and modeled carbon flux, model parameters, and particle size distribution (PSD) slopes during the BATS and DeepDOM field programs.

Cruise	Date	Depth	Deployment location	Deployment length (d)	Carbon flux replicates	POC flux (mmol m⁻² d⁻¹)	Modeled total POC flux (mmol m⁻² d⁻¹)	Modeled small POC flux (mmol m⁻² d⁻¹)	α (mmol C 300 μm particle⁻¹)	β (unitless)	PSD slope
BATS (NBSTs)	5 July 2013	150	31.7° N, 64.2° W	2.92	3	1.74 ± 0.63	1.73 ± 0.03	0.46 ± 0.01	$1.85 * 10^{-5}$	2.81	3.4
		300		2.86	3	0.75 ± 0.12	0.74 ± 0.02	0.35 ± 0.01			3.8
	1 Aug 2013	150	31.6° N, 64.2° W	2.45	2	1.79 ± 0.15	1.84 ± 0.07	1.24 ± 0.06	$1.62 * 10^{-5}$	2.03	3.5
		200		2.48	2	1.07 ± 0.14	1.05 ± 0.07	0.61 ± 0.06			2.9
		300		2.42	3	0.59 ± 0.12	0.57 ± 0.06	0.45 ± 0.05			4.0
	17 Sept 2013	150	31.7° N, 64.1° W	2.69	3	1.02 ± 0.21	0.63 ± 0.02	0.15 ± 0.01	$1.10 * 10^{-5}$	2.5	3.1
		300		2.67	3	0.55 ± 0.22	1.04 ± 0.02	0.37 ± 0.01			3.4
		500		2.70	3	0.65 ± 0.12	0.56 ± 0.02	0.35 ± 0.01			3.8
	19 Oct 2013	150	31.7° N, 64.2° W	2.65	3	0.88 ± 0.24	0.28 ± 0.01	0.071 ± 0.003	$6.22 * 10^{-6}$	2.88	3.2
		300		2.63	2	0.11 ± 0.32	0.22 ± 0.01	0.070 ± 0.003			3.2
		500		2.64	3	0.43 ± 0.28	0.34 ± 0.01	0.072 ± 0.003			3.5
	4 March 2014	150	31.6° N, 64.2° W	1.47	3	1.14 ± 0.35	1.09 ± 0.02	0.20 ± 0.005	$6.22 * 10^{-6}$	2.88	3.2
		300		1.48	3	0.92 ± 0.19	1.36 ± 0.02	0.33 ± 0.006			3.4
		500		1.45	2	0.97 ± 0.39	1.33 ± 0.02	0.35 ± 0.006			3.6
DeepDOM (surface-tethered, free floating)	28 March 2013	125	Station 2 38° S, 45° W	1.42	3	4.22 ± 0.69	–	–			3.0
	2 May 2013	125	Station 5 28.2° S, 38.5° W	0.90	3	3.86 ± 1.66	–	–			3.4
	2 May 2013	125	Station 5 28.2° S, 38.5° W	1.04	3	4.57 ± 0.94	–	–			3.0
	29 May 2013	125	Station 21 6.5° N, 48° W	0.73	1	2.55	–	–			3.3

at Station 5, 1 deployment at Station 21; Fig. 1, Table 1). Samples collected on the DeepDOM cruise were collected from surface-tethered, free-floating traps at 125 m deep.

To prepare the sediment traps onboard the ship, seawater was collected from a depth of 300 m on the BATS cruises and 500 m on the DeepDOM cruise in rosette-mounted Niskin bottles and was filtered through a 1 μm cartridge filter. Due to malfunction of the CTD rosette during the March 2014 BATS cruise, surface seawater was instead collected and filtered from the underway seawater collection system. Prior to deployment, trap tubes were filled with the filtered seawater, and 500 mL of formalin-poisoned brine (filtered seawater, 0.6 M NaCl, 0.1% formalin, 3 mM borate buffer) was added to the bottom through a tube. The salinity of the brine solution was approximately 70 ppt.

During the BATS cruises, each NBST was mounted with three trap tubes containing formalin brine and one trap tube containing a poly-acrylamide gel jar with overlying filtered seawater. In July and August 2013, NBSTs were deployed at depths of 150 m, 200 m, and 300 m and in September and October 2013 and March 2014 NBSTs were deployed at depths of 150 m, 300 m, and 500 m. All NBSTs remained within 10 m of their preprogrammed depths during deployment. Prior to recovery, the lids successfully closed on the NBSTs 54 out of 60 times, with 6 tubes remaining open on the first July cruise due to an error in the burn wire attachment. Additional trap tubes were identically prepared (1 brine, 1 gel) but kept in the ship's lab during the deployment period to serve as process blanks. On the DeepDOM cruise, three tubes containing formalin brine and one tube containing a gel jar with overlying seawater were attached to a metal frame, which was deployed at 125 m on a surface-tethered, free-floating trap array. Three tubes containing formalin brine with overlying seawater were kept on the ship as process blanks on three occasions between 28 March and 18 April 2013 during the DeepDOM cruise. The tops of all blank tubes were covered to prevent contamination from the air. Tubes used on the BATS and DeepDOM cruises were of identical construction and dimensions.

After recovery of the NBSTs and surface-tethered traps, trap tubes settled on the ship for at least 1 h before being processed. Overlying seawater was pumped from the top of the tube down to the brine interface or to the top of the gel jar. Gel jars were removed from the bottom of the trap tubes and the overlying seawater was gently siphoned off the top of the gel layer. Gels were stored at 4 °C until analysis. Brine was drained from the bottom of the trap tubes through a 350 μm mesh to remove zooplankton. Previous studies have shown that particles >350 μm are almost entirely composed of zooplankton that swam into the trap at BATS (Owens et al., 2012). Trap tubes and screens were rinsed with a small amount of filtered seawater to collect any small, adhered particles. Particles and screened zooplankton were collected by filtration onto separate, pre-combusted glass fiber filters (Whatman, Thermo Fisher Scientific Inc., USA). Particle-containing filters were stored at −20 °C until they were dried in a drying oven at 40–50 °C, then stored at room temperature until analysis. Process tube blanks were sampled and analyzed in the same way as deployed tubes.

2.3. Quantification of organic carbon flux

Dried glass fiber filters were pelletized into tin capsules in preparation for measurement of particulate carbon content. Samples collected during the 2013 BATS cruises were measured on a Flash EA1112 Carbon/Nitrogen Analyzer at the Woods Hole Oceanographic Institution Nutrient Analytical Facility. Samples collected during the 2014 March BATS cruises were measured at the Skidmore College Stable Isotope and Paleoclimate Analysis Laboratory using a Costech ECS 4010 elemental analyzer coupled to a ThermoScientific MAT 253 isotope ratio mass spectrometer via a Conflo IV interface. Acetanilide was used as the reference standard for mass calibration of both elements. Samples collected during the DeepDOM cruise were measured by the UC Davis Stable Isotope Facility on an Elementar elemental analyzer. The carbon

measured in all process blanks from BATS cruises (n = 5) was averaged together and the carbon measured in all process blanks from the DeepDOM cruise (n = 9) was averaged together to calculate the average background carbon in sediment trap tubes from each field program (9.2 ± 2.0 μmol C and 16.7 ± 3.6 μmol C respectively). The average carbon blank was subtracted from the measured carbon in trap samples before calculating flux. Particulate carbon flux was calculated from the blank-corrected carbon measured on each filter, normalized to the trap collection area (0.0113 m^2) and the duration of the collection period. The average particulate carbon flux was calculated from replicate trap tubes (Table 1). Four particulate carbon samples collected during the BATS cruises were lost during processing, so the averages of duplicate measurements are reported. Standard deviations were calculated when triplicate measurements were available, otherwise the range of duplicates is reported. At Station 21 in the tropical Atlantic, error is not reported because only one trap sample for carbon flux was collected.

2.4. Gel imaging

Particle containing gels were imaged using an Olympus SZX12 stereomicroscope with an Olympus Qcolor 5 camera attachment and QCapture imaging software. Particles were illuminated using fiber optic lights and images were captured at three magnifications (7×, 16×, 63×) to enable quantification of both the rare, large particles and the abundant, small particles. At a magnification of 7×, between 49% and 67% of the gel surface area was imaged in 16–22 fields of view in a single focal plane. At 16×, 17–38% of the gel surface area was imaged in randomly distributed fields of view across the entire gel surface. At this magnification, a single focal plane could not capture every particle within one field of view; large particles typically accumulated toward the bottom of the gel layer and relatively small particles were distributed in more focal planes throughout the gel layer. To reduce the underestimation of small particle abundance, two images were taken from different focal planes in each field of view (27–60 fields, 54–120 images). At 63×, 0.5–0.8% of the total gel surface area was imaged (12–20 fields of view). Images were taken in cross-sections spanning the diameter of the gel. The purpose of imaging a small percentage of the gel at high magnification was to accurately quantify the abundance of small particles. Between 11 and 15 focal planes were imaged in each field of view, depending on the depth of the gel and how many distinct focal planes contained particles. Imaging the same particle twice within one field of view was avoided by ensuring that focal planes did not include overlapping particles. Between 132 and 220 images were captured of each gel at 63× magnification. By imaging at three magnifications, between 240 and 360 images were captured of each gel.

2.5. Particle flux enumeration

Particles imaged in each gel at the same magnification were identified and measured using an analysis macro created using ImageJ software (Fig. 2). The macro iteratively applied a scale to each image (μm per pixel), subtracted the background, and converted the image color to 8-bit grayscale. The brightness was increased to a predefined level and a variance filter identified the edges of the in-focus particles. An automatic thresholding algorithm ("Intermodes") was applied to convert the image into a binary black-or-white image. The "Analyze Particles" tool identified each particle, measured the two-dimensional surface area, and recorded the image file name. All count data were subsequently analyzed using R software (R. Development Core Team, 2008).

Particles imaged from the same field of view but different focal planes were grouped together and the equivalent spherical diameter (ESD) of each particle in a field of view was calculated based on the measured two-dimensional surface area. Particles were divided into 26 base-2, log-spaced size classes ranging from 1 μm to 8192 μm based on their ESD. Counting error was calculated as the square root

of the number of particles counted in each size category. Size classes with 4 or fewer counted particles (≥50% error) were excluded from analysis. The abundance of particles in each size bin was calculated by normalizing the number of particles counted by the size bin width and by the analyzed gel surface area (Fig. 3A). The optimal magnification to calculate the abundance of a particle size category was defined as the magnification where the observed abundance most closely followed a power-law distribution (Fig. 3B). The abundance of 11–45 μm particles was quantified at 63× magnification, the abundance of 45–128 μm particles was quantified at 16× magnification, and the abundance of >128 μm particles was quantified at 7× magnification (Fig. 3B). Four
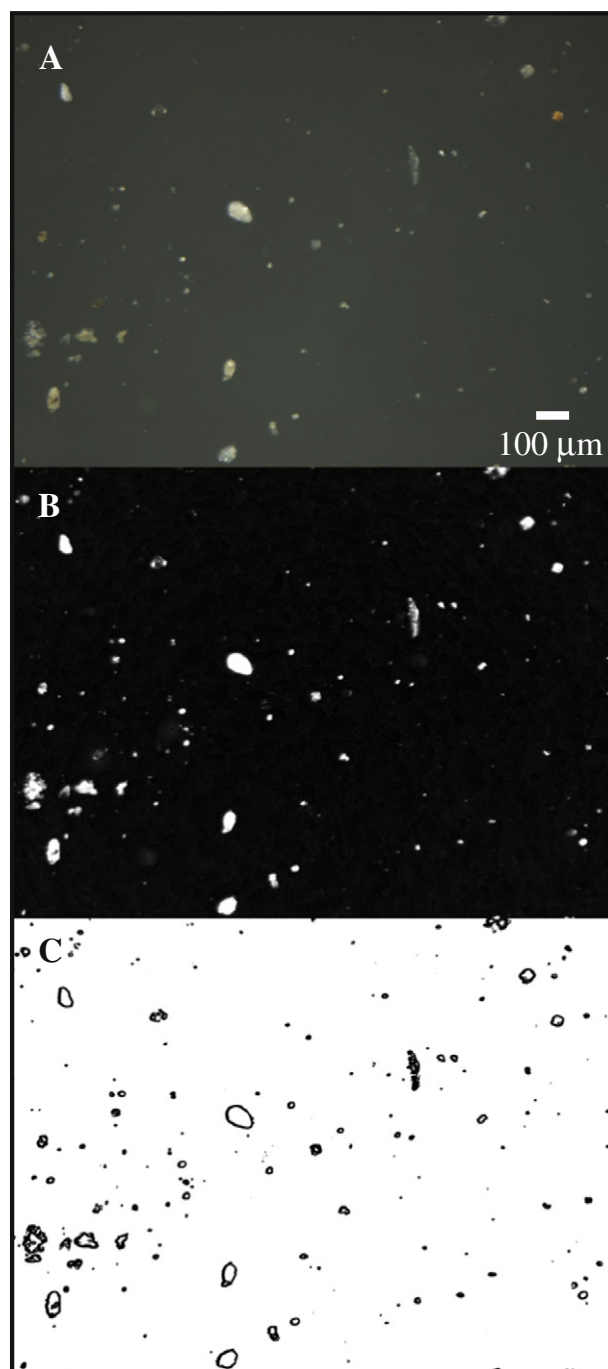

Fig. 2. Example of the image analysis protocol used to identify particles. A) Light micrograph of a gel taken at 63× magnification. B) Image after removal of background, conversion to gray scale, and brightness adjustment and C) after identification of edges, application of a threshold, and conversion to binary.

samples had slightly different size detection limits at each magnification and required different size ranges to quantify a power law distribution of particle abundance. This was likely due to small unavoidable changes in the lighting among samples. For the sample collected at 200 m in August, optimal particle size ranges were 11–64 μm (63×), 64–90 μm (16×), and >90 μm (7×). The optimal size ranges to calculate particle abundance from samples collected at 500 m in October and March were 11–45 μm (63×), 45–64 μm (16×), and >64 μm (7×). The optimal size ranges to calculate particle abundance in the sample from Station 21 collected during the DeepDOM cruise were 11–32 μm (63×), 32–128 μm (16×), and >128 μm (7×). The particle abundance in process blanks was subtracted from particle abundance in samples similar to the way process blanks were subtracted from particulate carbon measurements; the particle abundance of all five gel trap process blanks were measured and averaged together, and the average was subtracted from the particle abundance measured in each gel trap sample (Fig. 3C). No gel trap process blanks were available for the DeepDOM cruise, so the particle abundance measured in the process blanks during BATS cruises were subtracted from the abundance of particles in samples collected during the DeepDOM cruise. The particulate carbon process blanks were not significantly different between these cruises (p > 0.05), suggesting that DeepDOM gel trap blanks would have been similar to BATS gel trap blanks. Particle number flux was calculated by dividing blank-subtracted particle abundance by the trap deployment time (Fig. 3D).

2.6. Modeling particle size distributions

The slope of each particle size distribution (PSD) was calculated by fitting the observations of particle number flux to a differential power law size distribution model (Jackson et al., 1997),

$$PSD = A(ESD/ESD_r)^{-B} \qquad (1)$$

where A equals the number flux of particles in the smallest size category ESD_r (here 11–16 μm), and each size category (ESD) is normalized to ESD_r. B indicates the slope of the power law function; higher values have steeper slopes and a higher proportion of small particles relative to large particles. The "optim" function in R was used to identify the least-squares, best-fit values of A and B describing log-transformed particle number fluxes measured in each gel trap.

2.7. Modeling particle carbon content

The calculated carbon content of sinking particles was determined by the methods described by Alldredge (1998), further developed by Guidi et al. (2008b), and used previously at the BATS study location by McDonnell and Buesseler (2012). This method assumes that carbon content is directly related to particle volume and can be modeled as:

$$C_{particle} = \alpha(ESD/ESD_r)^{\beta}. \qquad (2)$$

The α parameter indicates the magnitude of the carbon content of particles with reference diameter ESD_r and the β parameter relates particle size to carbon content. In previous studies, the normalization to ESD_r was omitted, thus necessitating an unusual unit assignment for α (mmol C $\mu m^{-\beta}$) (McDonnell and Buesseler, 2012) or implicitly setting the reference diameter to 1 μm (Guidi et al., 2008b). However, a diameter of 1 μm is well below the observable size range for settling particles, which causes best-fit α values from different locations and times (Guidi et al., 2008b; Iversen et al., 2010; McDonnell and Buesseler, 2012) to vary across larger ranges than may be realistic. Here, the reference diameter was set to 300 μm, which is within the resolvable size range and is a size where settling particles are still numerically abundant. In this study, α values therefore represent the carbon content of 300 μm particles instead of 1 μm particles. The results of the carbon modeling
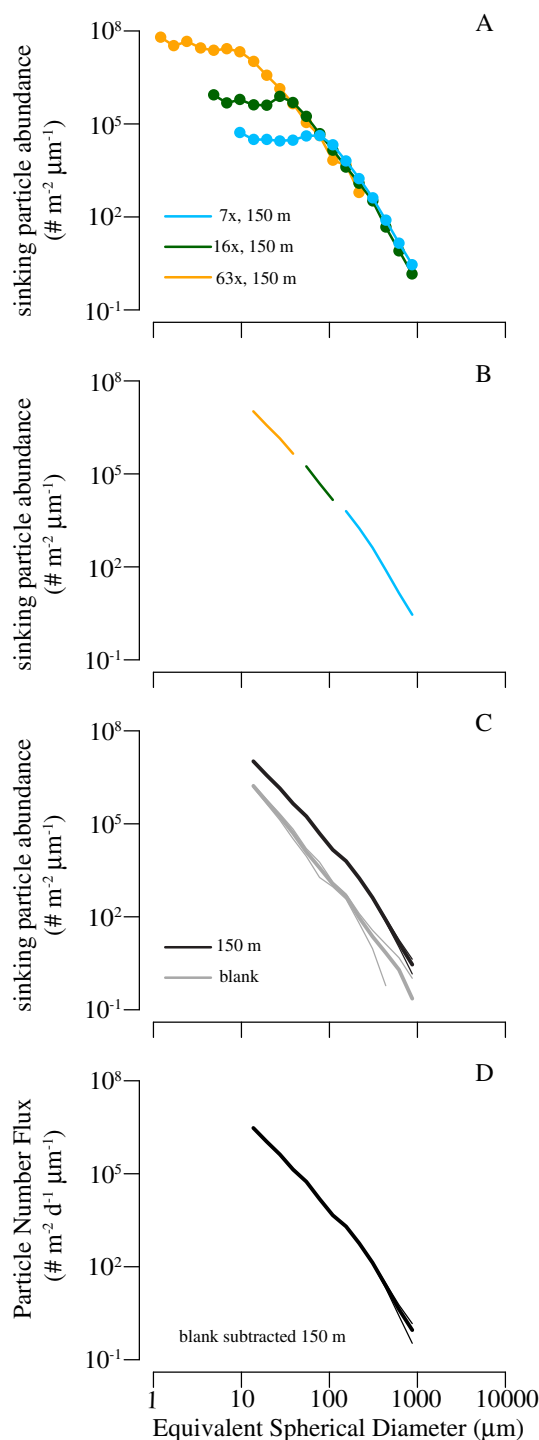

Fig. 3. Example of particle number flux analysis of a single gel trap collected during the BATS cruise in July 2013 from 150 m. A) Abundance of particle sizes quantified at three magnifications in the gel. B) Particle size range selected for quantification at each magnification. C) Composite of particle abundance for each particle size quantified at the optimal magnification in the sample and the average of the gel process blanks. The abundance of particles in the gel process blanks (gray) was subtracted from the abundance of particles in the sample (black). Thin lines indicate the upper and lower error estimates of counting uncertainty. D) Number flux of particles in the sample after subtracting the average abundance of particles detected in the gel blanks and dividing by deployment time.

equation are not affected by the value of the reference diameter, but including a reference diameter makes the units of the alpha value more meaningful. A β equal to 3 indicates a direct relationship of carbon content to particle volume, whereas a value smaller than 3 indicates that smaller particles contain more carbon relative to their size. The total

modeled carbon flux (mmol m^{-2} d^{-1}) is the sum across all particle size categories of $C_{particle}$ multiplied by the particle number flux:

$$C_{calc} = \Sigma \left(C_{particle(i)} \times F_i \times \Delta d_i \right) \qquad (3)$$

where $C_{particle(i)}$ is the carbon per particle of size category i, F_i is the particle number flux (number m^{-2} d^{-1} μm^{-1}) in the size category, and Δd_i is the bin width (μm) of the size category.

The "optim" function in R was used to identify the least-squares, best-fit values of α and β describing log-transformed carbon fluxes measured in trap tubes containing poisoned brine. Since 350 μm screens were used to remove the zooplankton that swam into the tubes used for carbon flux (Owens et al., 2012), only gel trap data from particles between 11–350 μm were included in the fit.

3. Results

3.1. Number flux of large and small particles

The particle number flux spectrum followed a typical power-law increase with decreasing particle size (McCave, 1975) down to a detection limit of 11 μm (Fig. 4). The abundance of particles observed at each magnification had a lower size limit of detection, defined as the size below which abundance remained constant with decreasing particle size (see where abundance distributions flatten out in Fig. 3A). The smallest observable size decreased with increasing magnification. The modeled slopes of the PSD (B value, Eq. (1)) were between 2.9 and 4 among all samples (Table 1). The slopes generally increased with increasing sample depth during each of the 5 months sampled at BATS, indicating an increase in the flux of small particles with depth relative to the flux of large particles (Fig. 5).

Identification of particles from gel image analysis resolved a large range of particle sizes, including sizes excluded in previous gel trap studies (<30 μm, Jackson et al., 2005; <73 μm McDonnell and Buesseler, 2010, 2012), and in situ particle imaging studies (<100 μm) (Guidi et al., 2008a). For the purposes of this study, we define 11–64 μm particles as "small" because in situ pump studies typically use 51 μm filters to separate large and small particles. The gel traps may also have collected

particles smaller than 11 μm, but these could not be accurately resolved by the techniques in this study. In the Sargasso Sea, the changes with depth of small particle flux often differed from large particle flux (Fig. 5). The flux of small particles increased with depth in July, September, and March, relative to the flux at 150 m, although the size range of small particles that increased with depth varied among months (see where number flux change crosses the dashed horizontal line in Fig. 5). The flux of larger particles consistently decreased with depth relative to flux at 150 m. In August, both large and small particle fluxes decreased with depth; the flux of small particles decreased at 200 m and the flux of all size classes decreased at 300 m depth. In October, no consistent change in flux with depth occurred across size categories.

3.2. Modeling carbon flux from sinking particle size distributions

At BATS, total measured carbon flux at all depths (150–500 m) ranged from 0.11 to 1.79 mmol C m^{-2} d^{-1}. The average carbon flux at 125 m in the South Atlantic and tropical Atlantic samples was nearly 3 times higher than the average carbon flux at 150 m at BATS (3.80 ± 0.88 mmol C m^{-2} d^{-1} vs. 1.31 ± 0.42 mmol C m^{-2} d^{-1}) (Table 1).

When a single set of carbon conversion parameters was determined for all 18 samples from BATS and DeepDOM cruises (α = 2.92 ∗ 10^{-6}, β = 1.82), modeled total carbon flux correlated with measured carbon flux (Pearson's r = 0.72, p < 0.05), mostly because of the large differences in measured carbon between BATS and DeepDOM samples (Fig. 6A). When a single set of carbon conversion parameters was determined for the 14 samples from BATS (Fig. 6B, α = 3.03 ∗ 10^{-6}, β = 1.81), the modeled values of total carbon flux were poorly correlated with measured carbon flux (Pearson's r = 0.15, p > 0.05). For this reason, optimal parameters for calculating the carbon content of particles were determined for each month at BATS separately. The function could not converge on optimal parameters for October or March BATS datasets individually, so these datasets were combined into a single parameterization. The correlation between modeled carbon flux using monthly parameters and the measured carbon flux was 0.83 (p < 0.001, Fig. 6C).

Best-fit α values to model the carbon content per particle at BATS (Eq. (2)) ranged between 6.22 × 10^{-6} in October/March and 1.85 × 10^{-5} in July. These values indicate an approximate 3-fold
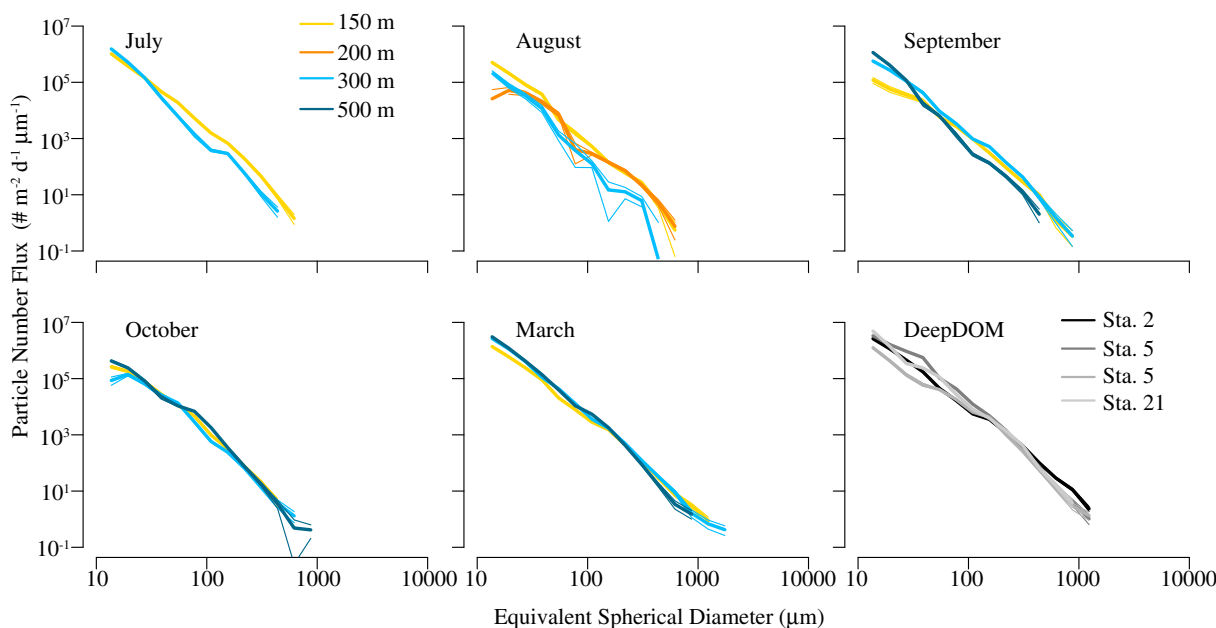

Fig. 4. Particle number flux distributions for all samples collected during 5 months at BATS and at 3 locations during the DeepDOM cruise. Thin lines indicate the upper and lower bounds of the counting uncertainty.
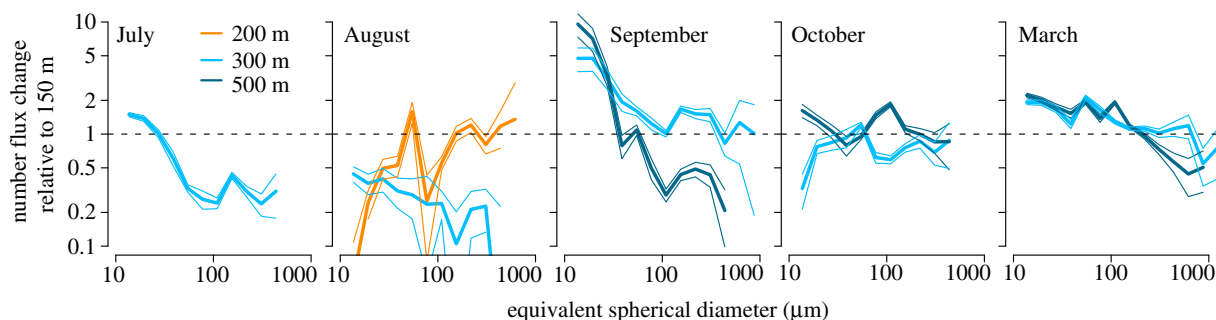
Fig. 5. Changes in particle number flux with depth at BATS during each sampling period. Changes at all depths are normalized to particle number flux at 150 m. Thin lines above and below represent the range of counting uncertainty. The horizontal dashed line at 1 indicates the location of no change relative to flux at 150 m.

increase in the modeled carbon content of 300 μm particles in July compared to October/March samples. Best-fit β values (Eq. (2)) ranged from 2.03 in August to 2.88 in October/March (Table 1). The difference in modeled β values suggests that in August large particles contained less carbon relative to their volume and that in other months carbon content was more closely related to particle volume. The large particles imaged in August appeared to have more fluid inclusions compared to other months and compared to smaller particles collected in August (Fig. 7). The qualitative change in particle composition across four locations and over 5 months at a single location (Fig. 7) suggest that the different parameters used to model carbon content at each sampling time represent real changes in particle characteristics across time and location. The model parameters were calculated based on data from particles smaller than 350 μm, although particles larger than this size cutoff were observed in the gel trap samples (Fig. 7).

The modeled total carbon flux at BATS was within the range of measured carbon flux at each depth sampled in July and August (Table 1). In September, October, and March the modeled total carbon flux was within the range of measured carbon flux in 5 out of the 9 samples collected. The modeled carbon flux by small particles ranged from 0.07 to 1.27 mmol C m^{-2} d^{-1} (Table 1). The modeled carbon transported by small particles decreased with depth in July and August, did not change with depth in October, and increased with depth in September and March. The percentage of total modeled carbon flux exported by small particles increased with depth during all months except in October (Fig. 8). In August, when some of the largest PSD slopes were observed (Table 1) and the large particles appeared to have increased fluid inclusions (Fig. 7), small particles were responsible for more than half of the modeled carbon flux. The average percentage of modeled carbon export by small particles at BATS was 39 ± 20% across all measurements, ranging between 18% and 78% depending on the depth and month.

4. Discussion

The collection of sinking particles as small as 11 μm, in sediment traps as deep as 500 m, demonstrates settling of non-aggregated small particles through at least some portion of the water column. During 3 out of 5 BATS cruises, the flux of large particles decreased with depth while the flux of small particles increased. One hypothesis to explain the source of small particles at depth is disaggregation or dissolution of large particles. Alternatively, small particles may slowly settle without aggregation, or be physically mixed or locally advected to depth. Our observations cannot address the primary mechanism that transported small particles to the depth at which they were captured, but they do indicate that small particles continue to sink at that depth regardless of the initial transport process.

The slopes of the number flux particle size distributions (between 2.9 and 4) were comparable to the slopes typically observed for particles suspended in the water column (Jackson et al., 1997; Sheldon et al., 1972; Stemmann and Boss, 2012). The slope of the particle number flux size distributions increased with depth, indicating the small particle flux increased with depth relative to large particle flux. Applying a single slope to the entire particle size spectrum may obscure small but significant departures from that slope between the smallest and the largest size ranges (Jackson et al., 1997; Stemmann et al., 2008). However, the increasing slope of the particle size distribution with depth accurately represents the observations; the number flux of small particles increased with depth while the number flux of large particles decreased with depth in 3 out of the 5 months sampled at BATS. These observations indicate that small particles are important contributors to flux throughout the water column and their contribution to flux often increases with depth at BATS.

In spite of their small size, small particles were responsible for approximately one third of the modeled carbon flux at 150 m in the Sargasso Sea
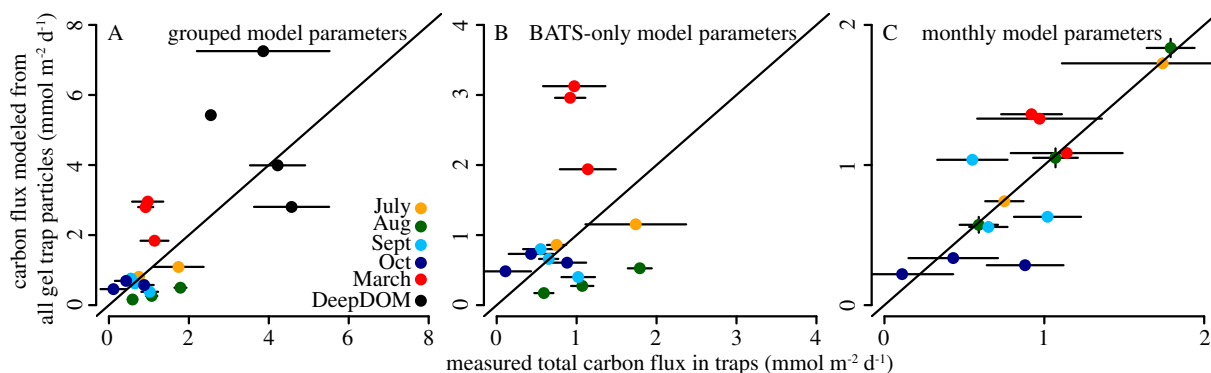

Fig. 6. Relationship of modeled carbon flux versus measured carbon flux when parameters is determined by A) combining all samples, B) combining only samples collected at BATS, and C) separating samples collected at BATS by month, with only October and March samples combined together. Vertical error bars indicate the uncertainty due to counting error (smaller than symbols). Horizontal error bars indicate the standard deviation of triplicate or range of duplicate carbon flux measurements (see Table 1). Diagonal line indicates the 1:1 relationship between modeled and measured flux.
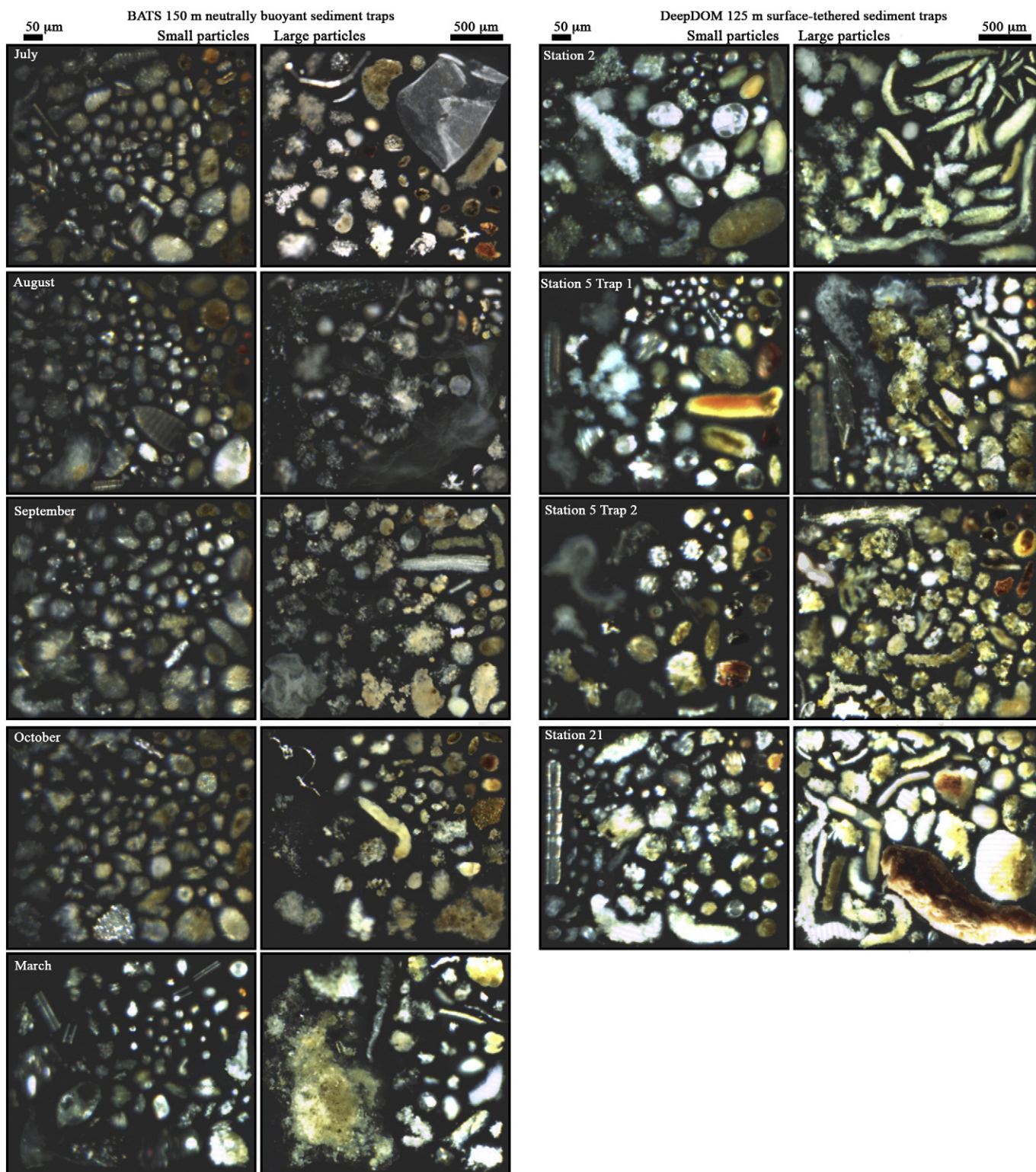
Fig. 7. Examples of sinking particles captured during BATS (left two columns) and DeepDOM (right two columns) cruises. Mosaics of micrographs include particles collected at 150 m (BATS) or 125 m (DeepDOM). Micrographs of small particles were captured at 63× magnification and micrographs of large particles were captured at 16× magnification and minimally altered to create the mosaic (only the background around each particle was removed). To illustrate a representative assortment of particles, most of the distinguishable particles from the first 8 fields of view (63×) or 18 fields of view (16×) were included in the mosaic.

on average and that fraction typically increased with depth. The data indicates that small particles are an important component of carbon export from the surface and become relatively more important with depth. In August, small particles were responsible for 67% of the carbon export out of the surface, indicating that small particles can be responsible for

the majority of carbon export during certain time periods. More frequent and long-term observations are needed to determine how often this occurs.

Riley et al (2012) found that small and/or slowly sinking particles were responsible for 63% of the carbon sinking from the surface at one
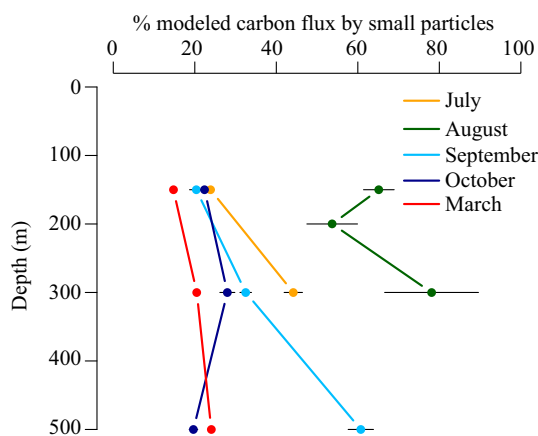
Fig. 8. Percentage of the modeled carbon flux exported by small particles (11–64 μm) during five BATS cruises. Color of lines corresponds to the month of sample collection. Error bars indicate the uncertainty due to counting error.

location in the North Atlantic, but hypothesized that this contribution would diminish with depth because most of the small and/or slowly sinking particles would be remineralized. Instead, we observed an increasing contribution of small particles to flux at depth, in spite of remineralization. Carbon flux observational strategies and models of the biological pump that neglect small, settling particles may have attenuation rates that are too large, and remineralization depths that are too shallow.

The importance of small particle sizes to carbon flux and their attenuation with depth was determined by modeling the carbon content of different particle sizes (Eq. (2)). Although they are extremely abundant, the per-particle carbon content of small particles could be small, and therefore their contribution to carbon export could be negligible. The parameterization of carbon content used in this study assumes that carbon content is a power-law function of particle diameter, and the modeled contribution of small size classes to carbon flux is sensitive to the value of β (Eq. (2)). The model does not account for the diversity of particle types that are represented within a single size category, or changes in the character of the sinking particles with depth. We made an effort to reduce month-to-month and location variability in the model parameters by determining them separately for each month and field program where possible. This improved the correspondence between the modeled and measured carbon values.

McDonnell and Buesseler (2012) recognized the variability in carbon conversion parameters and found that the carbon flux they observed at the BATS location was not accurately described by parameters determined at other field locations. The β-value calculated for samples collected at BATS by McDonnell and Buesseler (2012) was 3.24, which is larger than the β-value calculated in the present study (β ranging 2.03-2.88; Table 1). The difference in parameters could be due to natural variability in the relative carbon content over time. The present study also quantified a larger size range of particles, which may also have contributed to differences in parameter values. Similar to this study, Alldredge (1998) identified β parameters less than 3, indicating that large particles contain less carbon relative to their volume, a characteristic of large aggregates with less densely packed organic matter and more fluid inclusion.

The α value in the present study is not comparable to those in previous studies because here we normalize particle ESD to a reference diameter of 300 μm instead of 1 μm. This produced less variation in the α values among sample sets, and the amount of variation (approximately a factor of 3, rather than orders of magnitude) was more intuitively consistent with possible natural variations in the carbon content of particles. In future studies, the accuracy of the power law model for particle carbon content could be better validated if the carbon content of

individual particles could be directly measured. If such a method were available, the model could be better constrained because it would not solely rely on the comparison of total modeled carbon flux to total measured carbon flux.

Carbon export by small particles is not limited to low flux environments where small cells and particles dominate the ecosystem. Higher total carbon flux was observed at locations in the South Atlantic during the DeepDOM cruise, and small particles also contributed to carbon export at these locations. A robust parameterization of particle carbon content was not possible for these high flux locations, but the high abundance of small particles in higher flux environments suggests that small particles may also account for a large percentage of carbon export as these locations. More samples are needed to determine the relative influence of small particles in high and low flux environments.

Different trapping methods used to collect particles during the BATS cruises versus during the DeepDOM cruise may also have caused changes in the composition of particles collected during the field programs. NBSTs are particularly well suited for collecting small and potentially slowly sinking particles because they are designed to reduce the hydrodynamic bias of particle collection (Valdes and Price, 2000). The surface-tethered, free-floating traps used on the DeepDOM cruise may have been influenced by hydrodynamic biases that may under-collect slowly sinking particles (Buesseler et al., 2000, 2007a; Gardner, 1985). If so, the flux of small particles measured during the DeepDOM cruise would be underestimated. Surface tethered traps were also used in the gel trap study by McDonnell and Buesseler (2012) at BATS, and may also have under-collected small and slowly sinking particles. This may also have contributed to the differences in modeled carbon conversion parameters from the present study. Thus, differences in trapping efficiency also need to be considered when comparing datasets. However, Owens et al. (2012) found not consistent differences between carbon captured by the two sediment trap types, and suggested that sample processing methods may influence measurements more than trap type.

This study was able to detect a larger size range of settling particles than reported in earlier studies through use of gel collectors on NBSTs, and imaging the gels at both low and high magnification. Jackson et al. (2005) used a similar method and also observed improvements in the accuracy of small particle quantification (down to ~30 μm) when higher magnifications were used to image the gels. Presumably particles even smaller than those identified in the present study could be quantified under higher magnification. In future studies, small particles will be easier to identify and quantify in fewer focal planes if gel layers are thinner, and if collection containers can be made compatible with high-powered microscopes. Alternatively, Waite et al. (2000) physically isolated particles from the gel and imaged them by confocal microscopy to identify the picoplankton contents inside large sinking aggregates and fecal pellets collected in gel traps. Gel traps enable interrogation of the individual sinking particles responsible for carbon export and resolution of their individual characteristics. In this study, the use of gel traps revealed an important contribution of small particles to carbon flux, and future studies could be designed to observe the nature of these small particles and the mechanisms that lead to their transport through the mesopelagic.

References

Alldredge, A., 1998. The carbon, nitrogen and mass content of marine snow as a function of aggregate size. Deep-Sea Res. I Oceanogr. Res. Pap. 45, 529–541. http://dx.doi.org/10.1016/S0967-0637(97)00048-4.

Alonso-González, I.J., Arístegui, J., Lee, C., Sanchez-Vidal, A., Calafat, A., Fabrés, J., Sangrá, P., Masqué, P., Hernández-Guerra, A., Benítez-Barrios, V., 2010. Role of slowly settling particles in the ocean carbon cycle. Geophys. Res. Lett. 37, L13608. http://dx.doi.org/10.1029/2010GL043827.

Buesseler, K.O., Boyd, P.W., 2009. Shedding light on processes that control particle export and flux attenuation in the twilight zone of the open ocean. Limnol. Oceanogr. 54, 1210.

Buesseler, K.O., Steinberg, D.K., Michaels, A.F., Johnson, R.J., Andrews, J.E., Valdes, J.R., Price, J.F., 2000. A comparison of the quantity and composition of material caught in a neutrally buoyant versus surface-tethered sediment trap — origins and biological components. Deep-Sea Res. I Oceanogr. Res. Pap. 47, 277–294. http://dx.doi.org/10.1016/S0967-0637(99)00056-4.

Buesseler, K.O., Lamborg, C.H., Boyd, P.W., Lam, P.J., Trull, T.W., Bidigare, R.R., Bishop, J.K.B., Casciotti, K.L., Dehairs, F., Elskens, M., Honda, M., Karl, D.M., Siegel, D.A., Silver, M.W., Steinberg, D.K., Valdes, J., Van Mooy, B., Wilson, S., 2007a. Revisiting carbon flux through the ocean's twilight zone. Science 316, 567–570.

Buesseler, K.O., Antia, A.N., Chen, M., Fowler, S.W., Gardner, W.D., Gustafsson, O., Harada, K., Michaels, A.F., van der Loeff, M.R., Sarin, M., Steinberg, D.K., Trull, T., 2007b. An assessment of the use of sediment traps for estimating upper ocean particle fluxes. J. Mar. Res. 65, 345–416.

Burd, A.B., Jackson, G.A., 2009. Particle aggregation. Annu. Rev. Mar. Sci. 1, 65–90. http://dx.doi.org/10.1146/annurev.marine.010908.163904.

Close, H.G., Shah, S.R., Ingalls, A.E., Diefendorf, A.F., Brodie, E.L., Hansman, R.L., Freeman, K.H., Aluwihare, L.I., Pearson, A., 2013. Export of submicron particulate organic matter to mesopelagic depth in an oligotrophic gyre. Proc. Natl. Acad. Sci. 110, 12565–12570.

Dall'Olmo, G., Mork, K.A., 2014. Carbon export by small particles in the Norwegian Sea. Geophys. Res. Lett. 41, 2921–2927. http://dx.doi.org/10.1002/2014GL059244.

De La Rocha, C.L., Passow, U., 2007. Factors influencing the sinking of POC and the efficiency of the biological carbon pump. Deep-Sea Res. II Top. Stud. Oceanogr. 54, 639–658.

Ebersbach, F., Trull, T., 2008. Sinking particle properties from polyacrylamide gels during the KErguelen Ocean and Plateau compared Study (KEOPS): zooplankton control of carbon export in an area of persistent natural iron inputs in the Southern Ocean. Limnol. Oceanogr. 53, 212–224.

Fowler, S.W., Knauer, G.A., 1986. Role of large particles in the transport of elements and organic compounds through the oceanic water column. Prog. Oceanogr. 16, 147–194. http://dx.doi.org/10.1016/0079-6611(86)90032-7.

Gardner, W.D., 1985. The effect of tilt on sediment trap efficiency. Deep Sea Res. Part A Oceanogr. Res. Pap. 32, 349–361.

Gardner, W.D., Chung, S.P., Richardson, M.J., Walsh, I.D., 1995. The oceanic mixed-layer pump. Deep-Sea Res. II Top. Stud. Oceanogr. 42, 757–775.

Giering, S.L.C., Sanders, R., Lampitt, R.S., Anderson, T.R., Tamburini, C., Boutrif, M., Zubkov, M.V., Marsay, C.M., Henson, S.A., Saw, K., Cook, K., Mayor, D.J., 2014. Reconciliation of the carbon budget in the ocean's twilight zone. Nature 507, 480–483.

Guidi, L., Gorsky, G., Claustre, H., Miquel, J.C., Picheral, M., Stemmann, L., 2008a. Distribution and fluxes of aggregates >100 μm in the upper kilometer of the South-Eastern Pacific. Biogeosciences 5, 1361–1372.

Guidi, L., Jackson, G.A., Stemmann, L., Miquel, J.C., Picheral, M., Gorsky, G., 2008b. Relationship between particle size distribution and flux in the mesopelagic zone. Deep-Sea Res. I Oceanogr. Res. Pap. 55, 1364–1374. http://dx.doi.org/10.1016/j.dsr.2008.05.01.

Guidi, L., Stemmann, L., Jackson, G.A., Ibanez, F., Claustre, H., Legendre, L., Picheral, M., Gorsky, G., 2009. Effects of phytoplankton community on production, size, and export of large aggregates: a world-ocean analysis. Limnol. Oceanogr. 54, 1951–1963.

Iversen, M.H., Nowald, N., Ploug, H., Jackson, G.A., Fischer, G., 2010. High resolution profiles of vertical particulate organic matter export off Cape Blanc, Mauritania: degradation processes and ballasting effects. Deep-Sea Res. I Oceanogr. Res. Pap. 57, 771–784. http://dx.doi.org/10.1016/j.dsr.2010.03.007.

Jackson, G.A., Burd, A.B., 1998. Aggregation in the marine environment. Environ. Sci. Technol. 32, 2805–2814. http://dx.doi.org/10.1021/es980251w.

Jackson, G.A., Maffione, R., Costello, D.K., Alldredge, A.L., Logan, B.E., Dam, H.G., 1997. Particle size spectra between 1 μm and 1 cm at Monterey Bay determined using multiple instruments. Deep-Sea Res. I Oceanogr. Res. Pap. 44, 1739–1767.

Jackson, G.A., Waite, A.M., Boyd, P.W., 2005. Role of algal aggregation in vertical carbon export during SOIREE and in other low biomass environments. Geophys. Res. Lett. 32, L13607.

Jacobs, M.B., Thorndike, E.M., Ewing, M., 1973. A comparison of suspended particulate matter from nepheloid and clear water. Mar. Geol. 14, 117–128. http://dx.doi.org/10.1016/0025-3227(73)90055-8.

Lundsgaard, C., 1995. Use of high viscosity medium in studies of aggregates, sediment trap studies in the Nordic countries. 3. Proceedings of the Symposium on Seasonal Dynamics of Planktonic Ecosystems and Sedimentation in Coastal Nordic Waters. Finnish Environment Agency.

McCave, I.N., 1975. Vertical flux of particles in the ocean. Deep Sea Res. Oceanogr. Abstr. 22, 491–502. http://dx.doi.org/10.1016/0011-7471(75)90022-4.

McDonnell, A.M., Buesseler, K., 2010. Variability in the average sinking velocity of marine particles. Limnol. Oceanogr. 55, 2085–2096.

McDonnell, A.M., Buesseler, K.O., 2012. A new method for the estimation of sinking particle fluxes from measurements of the particle size distribution, average sinking velocity, and carbon content. Limnol. Oceanogr. Methods 10, 329–346.

Michaels, A.F., Silver, M.W., 1988. Primary production, sinking fluxes and the microbial food web. Deep Sea Res. Part A Oceanogr. Res. Pap. 35, 473–490. http://dx.doi.org/10.1016/0198-0149(88)90126-4.

Owens, S., Buesseler, K., Lamborg, C., Valdes, J., Lomas, M., Johnson, R., Steinberg, D., Siegel, D., 2012. A new timeseries of particle export from neutrally buoyant sediment traps at the Bermuda Atlantic Time-series Study site. Deep-Sea Res. I Oceanogr. Res. Pap. 73, 34–47.

R. Development Core Team, 2008. R: A Language and Environment for Statistical Computing. R Foundation for Statistical Computing, Vienna, Austria.

Richardson, T.L., Jackson, G.A., 2007. Small phytoplankton and carbon export from the surface ocean. Science 315, 838–840.

Riley, J.S., Sanders, R., Marsay, C., Le Moigne, F.A.C., Achterberg, E.P., Poulton, A.J., 2012. The relative contribution of fast and slow sinking particles to ocean carbon export. Glob. Biogeochem. Cycles 26, GB1026. http://dx.doi.org/10.1029/2011GB004085.

Sheldon, R.W., Prakash, A., Sutcliffe, W.H., 1972. The size distribution of particles in the ocean. Limnol. Oceanogr. 17, 327–340.

Siegel, D.A., Buesseler, K.O., Doney, S.C., Sailley, S.F., Behrenfeld, M.J., Boyd, P.W., 2014. Global assessment of ocean carbon export by combining satellite observations and food-web models. Glob. Biogeochem. Cycles http://dx.doi.org/10.1002/2013GB004743 (GB004743).

Silver, M.W., Gowing, M.M., 1991. The "particle" flux: origins and biological components. Prog. Oceanogr. 26, 75–113. http://dx.doi.org/10.1016/0079-6611(91)90007-9.

Stemmann, L., Boss, E., 2012. Plankton and particle size and packaging: from determining optical properties to driving the biological pump. Ann. Rev. Mar. Sci. 4, 263–290.

Stemmann, L., Jackson, G.A., Gorsky, G., 2004a. A vertical model of particle size distributions and fluxes in the midwater column that includes biological and physical processes—part II: application to a three year survey in the NW Mediterranean Sea. Deep-Sea Res. I Oceanogr. Res. Pap. 51, 885–908. http://dx.doi.org/10.1016/j.dsr.2004.03.002.

Stemmann, L., Jackson, G.A., Ianson, D., 2004b. A vertical model of particle size distributions and fluxes in the midwater column that includes biological and physical processes—part I: model formulation. Deep-Sea Res. I Oceanogr. Res. Pap. 51, 865–884. http://dx.doi.org/10.1016/j.dsr.2004.03.001.

Stemmann, L., Eloire, D., Sciandra, A., Jackson, G.A., Guidi, L., Picheral, M., Gorsky, G., 2008. Volume distribution for particles between 3.5 to 2000 μm in the upper 200 m region of the South Pacific Gyre. Biogeosciences 5.

Trull, T.W., Bray, S.G., Buesseler, K.O., Lamborg, C.H., Manganini, S., Moy, C., Valdes, J., 2008. In situ measurement of mesopelagic particle sinking rates and the control of carbon transfer to the ocean interior during the Vertical Flux in the Global Ocean (VERTIGO) voyages in the North Pacific. Deep-Sea Res. II Top. Stud. Oceanogr. 55, 1684–1695.

Valdes, J.R., Price, J.F., 2000. A neutrally buoyant, upper ocean sediment trap. J. Atmos. Ocean. Technol. 17, 62–68. http://dx.doi.org/10.1175/1520-0426(2000)017<0062:ANBUOS>2.0.CO;2.

Volk, T., Hoffert, M., 1985. Ocean carbon pumps: analysis of relative strengths and efficiencies in ocean-driven atmospheric CO₂ changes. Geophys. Monogr. Ser. 32, 99–110.

Waite, A.M., Safi, K.A., Hall, J.A., Nodder, S.D., 2000. Mass sedimentation of picoplankton embedded in organic aggregates. Limnol. Oceanogr. 45, 87–97.

Woodward, G., Ebenman, B., Emmerson, M., Montoya, J.M., Olesen, J.M., Valido, A., Warren, P.H., 2005. Body size in ecological networks. Trends Ecol. Evol. 20, 402–409. http://dx.doi.org/10.1016/j.tree.2005.04.005.